Published in final edited form as:
J Biomech. 2014 June 27; 47(9): 2088–2094. doi:10.1016/j.jbiomech.2013.12.021.

Elastic, Permeability and Swelling Properties of Human Intervertebral Disc Tissues: A Benchmark for Tissue engineering

Daniel H. Cortes[1], **Nathan T. Jacobs**[2], **John F. DeLucca**[1], and **Dawn M. Elliott**[1,*]

[1] Department of Biomedical Engineering University of Delaware, Newark, DE

[2] Department of Mechanical Engineering University of Pennsylvania, Philadelphia, PA

SUMMARY

The aim of functional tissue engineering is to repair and replace tissues that have a biomechanical function, i.e., connective orthopaedic tissues. To do this, it is necessary to have accurate benchmarks for the elastic, permeability, and swelling (i.e., biphasic-swelling) properties of native tissues. However, in the case of the intervertebral disc, the biphasic-swelling properties of individual tissues reported in the literature exhibit great variation and even span several orders of magnitude. This variation is probably caused by differences in the testing protocols and the constitutive models used to analyze the data. Therefore, the objective of this study was to measure the human lumbar disc annulus fibrosus (AF), nucleus pulposus (NP), and cartilaginous endplates (CEP) biphasic-swelling properties using a consistent experimental protocol and analyses. The testing protocol was composed of a swelling period followed by multiple confined compression ramps. To analyze the confined compression data, the tissues were modeled using a biphasic-swelling model, which augments the standard biphasic model through the addition of a deformation-dependent osmotic pressure term. This model allows considering the swelling deformations and the contribution of osmotic pressure in the analysis of the experimental data. The swelling stretch was not different between the disc regions (AF: 1.28±0.16; NP: 1.73±0.74; CEP: 1.29±0.26), with a total average of 1.42. The aggregate modulus (Ha) of the matrix was higher in the CEP (390 kPa) compared to the NP (100 kPA) or AF (30 kPa). The permeability was very different across tissues regions, with the AF permeability (80 E^{-4} mm^4/Ns) higher than the NP and CEP (6-7 E^{-16} m^4/Ns). Additionally, a normalized time-constant (3000 sec) for the stress relaxation was similar for all the disc tissues. The properties measured in this study are important as benchmarks for tissue engineering and for modeling the disc's mechanical behavior and transport.

* Corresponding Author: Dawn M. Elliott, Ph.D. University of Delaware Department of Biomedical Engineering 125 E Delaware Ave. Newark, DE 19716 delliott@udel.edu.

CONFLICT OF INTEREST
The authors do not have any conflict of interests to disclose

INTRODUCTION

The function of the intervertebral disc is to transmit spine loads while allowing relative motion between the vertebral bodies. However, the function of the intervertebral disc is impaired by disc degeneration, a cascade of compositional and structural changes, that often results in low back pain (Adams and Dolan, 2012; Adams and Roughley, 2006; Urban and Roberts, 2003). Surgical treatments of painful disc degeneration include fusion of the vertebral bodies and arthroplasty, which alleviate symptoms but do not restore the disc structure or function. Tissue engineered disc replacements are promising alternatives to current surgical approaches (Hudson et al., 2013). Engineered discs can potentially restore both the native structure and function while preserving the capacity of the disc to remodel in response to external stimuli (Bowles et al., 2012; Hudson et al., 2013; Lee et al., 2012; Mizuno et al., 2006; Nerurkar et al., 2010b; Xin et al., 2013). To provide a similar function compared to native intervertebral disc, tissue engineered replacements must have similar mechanical behavior as healthy intervertebral discs (Nerurkar et al., 2010a).

The mechanical behavior of the intervertebral disc is a product of the biphasic-swelling properties (defined as the elastic, permeability, and swelling properties) of its individual tissue components: the annulus fibrosus (AF), nucleus pulposus (NP), and cartilaginous endplate (CEP) (Cortes and Elliott, 2014). Measuring the biphasic-swelling properties of the individual disc tissues is important as benchmarks for tissue engineering and for modeling the disc's mechanical behavior and transport. The tensile mechanical behavior of the fiber-reinforced AF has been extensively studied and accurately described using constitutive models (Guerin and Elliott, 2007; Guo et al., 2012; Klisch and Lotz, 1999; O'Connell et al., 2012; Sen et al., 2012; Wagner and Lotz, 2004; Wagner et al., 2006; Wu and Yao, 1976). However, mechanical properties of the human AF extra-fibrillar matrix have been less explored, and the reported values for permeability span several orders of magnitude (Table 1). This variation in permeability is probably caused by differences in the testing protocols and the constitutive models used to analyze the data. Additionally, limited data are available for elastic properties and permeability of the human NP and CEP (Table 1). Osmotic swelling plays a crucial role on the hydration and function of the intervertebral disc, but has received little consideration in the measurement of tissues properties. Therefore, the objective of this study was to measure the human lumbar disc AF, NP, and CEP biphasic-swelling properties using a consistent experimental protocol and analyses.

METHODS

The biphasic-swelling properties the AF, NP and CEP were measured using confined compression experiments. The testing protocol was composed of a swelling period followed by multiple compression ramps. Similarly, the analysis of the experimental data was divided in two steps: one to calculate the swelling stretch, and another to calculate the tissue properties from the transient response of the applied compression strains.

Sample Preparation

14 lumbar spines were acquired from an approved vendor (NDRI, Philadelphia, PA), the age range of the donors was between 43 and 93 years old, and the gender distribution was 11

male and 3 female donors. Spines were imaged in a 3 Tesla scanner to determine the degenerative grade using a protocol established in previous studies (Cortes et al., 2013; O'Connell et al., 2012). All the tested discs had a degeneration grade of 3 or lower. Samples from discs with grades 4 and 5 could not be successfully dissected or tested and therefore were not included in the study. AF samples were dissected from three locations in the mid-sagittal plane of L3-L4 intervertebral discs: posterior (PAF, n=6), outer-anterior (OAF, n = 7) and inner-anterior (IAF, n = 5). The axis of the AF samples was perpendicular to the lamellae (radial direction) to minimize fiber contribution during the compression test. CEP and NP samples were dissected from discs at different levels of the lumbar spine (L1-L2: n = 5; L2-L3: n = 6; L3-L4: n = 1) (Figure 1). The samples were sectioned on a freezing-stage microtome to a thickness of 1.5 mm for AF and NP samples, and 0.8 mm for CEP. A plug of 4 mm in diameter was excised using a biopsy punch.

Confined Compression Protocol

The confined compression protocol consisted of a swelling period of 3 hours, where the samples were allowed to equilibrate within a PBS bath, followed by a series of compression-relaxation ramps that were held to allow for stress-relaxation to equilibrium. For AF samples, the initial swelling was performed outside the testing chamber and the sample was then placed in the testing device (Instron 5542, Canton, MA) and thickness was measured after reaching equilibrium under a 1 kPa preload (Cortes et al., 2013). Five compression ramps of 10% were then applied in a period of 2000 seconds (strain rate of 0.005%/s), followed by relaxation periods ranging from 2 to 6 hours.

To avoid over-hydration of the NP and CEP samples, the initial swelling was performed while contained in the confined compression chamber (isometric swelling). Although no change in volume is experienced during the isometric swelling period, osmotic swelling results in a pressurization of the confined compression chamber (Johannessen and Elliott, 2005; Périé et al., 2005). After isometric swelling, 3 compression ramps of 5% of the initial thickness were applied in a period of 300 seconds (i.e. strain rate of 0.016%/s,) followed by relaxation periods of 4000, 6000 and 8000 seconds for NP samples, and 3000, 3000 and 4000 seconds for CEP samples. Preliminary experiments showed that these relaxation periods were sufficient to reach equilibrium.

Water and glycosaminoglycan content

Water and GAG content for AF tissue was measured only for tested samples (Cortes et al., 2013). A previous study on bovine AF showed no differences in fixed charge density between tested samples and adjacent tissue (Cortes and Elliott, 2011). However, since no preliminary data was available for NP and CEP, water and GAG content of NP and CEP were measured in adjacent tissue and tested samples following completion of the mechanical testing. The water content was determined by the difference between wet and dry weight. Samples were digested overnight in a papain solution (2% vol) at 65 °C. Glycosamiglycan content was measured using a 1,9-dimethylmethylene blue (DMMB) assay with chondroitin-6-sulfate as the standard and expressed as percentage of dry weight (Han et al., 2012; Jacobs et al., 2011; Nerurkar et al., 2011).

Biphasic-Swelling Model

To analyze the confined compression data, the tissues were modeled using a biphasic-swelling model. This model augments the standard biphasic model through the addition of a deformation-dependent osmotic pressure term (Ehlers et al., 2009; Galbusera et al., 2011; Wilson et al., 2005). This model is a simplification of the triphasic theory because it assumes that the ion concentration is in equilibrium at all times. Therefore the ion concentration and the osmotic pressure only depend on the fixed charge density and the external ion concentration. In the biphasic-swelling model, the applied stress is defined as the addition of the fluid and osmotic pressure (p_f and p_{os}) and the matrix stress ($\boldsymbol{\sigma}_{matrix}$):

$$\boldsymbol{\sigma} = -(\mathbf{p_f} + \mathbf{p_{os}})\,\mathbf{I} + \boldsymbol{\sigma}_{\mathbf{matrix}} \quad (1)$$

At equilibrium, such as the end of the relaxation period after a compression ramp, the fluid pressure, p_f, is zero, and the applied stress is the addition of the matrix stress and the osmotic pressure. The expression for the osmotic pressure assuming ideal solutions is presented in Eq. (2) and the constitutive equation for the matrix in terms of the strain energy functions is presented in Eq (3).

$$p_{os} = RT\left(\sqrt{c_{fc}^2 - 4c_b^2} - 2c_b\right), \quad (2)$$

$$\Psi^{matrix} = \frac{C_1}{I_3^{\beta}} e^{[C_2(I_1-3)+C_3(I_2-3)]}, \quad (3)$$

where, R is the universal gas constant, T is the absolute temperature, c_{fc} is the fixed charge density, c_b is the ion concentration in the testing bath, C_i (i = 1, 2, 3) are material properties, I_1, I_2, and I_3 are strain invariants and $\beta = C_2 + 2C_3$. The Holmes-Mow model used for the matrix is defined by three parameters: C_1, C_2 and C_3; where C_1 represents the stiffness of the tissue in the reference configuration, while C_2 and C_3 control the non-linearity (Holmes and Mow, 1990). The parameters C_1, C_2 and C_3 are related to Poisson's ratio (ν), Young modulus (E) and Aggregate compression modulus (Ha) and by the expressions:

$$v = \frac{C_3}{C_2 + 3C_3}, \quad E = 4C_1(C_2 + C_3)(1+v), \quad Ha = \frac{4C_1(C_2+C_3)(1-v)}{1-2v}. \quad (4)$$

Deformation of the solid matrix, which is caused by either the external applied forces or the osmotic pressure, alters the tissue volume and the fixed charge density (c_{fc}). This change can be quantified using

$$c_{fc} = \frac{c_{fc0}\phi_f^0}{\left(J - 1 + \phi_f^0\right)} \quad (5)$$

where c_{fc0} and ϕ_f^0 are the fixed charge density and the water content, respectively, at the reference configuration; and J is the ratio between the volume at the deformed and reference

configuration. The fixed charge density in the reference configuration was calculated from the GAG content as (Chahine et al., 2004):

$$c_{fc0}=Z_{cs}c_{GAG}/M_{cs} \quad (6)$$

where c_{GAG} is mg of GAG per ml of water, and M_{CS} and Z_{CS} are the molecular weight and number of charges per CS disaccharide, respectively (Z_{CS} = 2 charges/repeating unit; M_{CS}=513 g/repeating unit). For NP and CEP tissues, the average fixed charge density of the tested sample and the corresponding adjacent tissue was used for the curve fitting process.

The permeability was assumed to be strain dependent with the following constitutive relation (Holmes and Mow, 1990):

$$k=k_0\left(\frac{J-\phi_f^0}{1-\phi_f^0}\right)^2 e^{-M(I_3-1)/2} \quad (7)$$

where k_0 is the hydraulic permeability in the reference configuration, and M is a non-linear parameter.

In confined compression, the rate of stress relaxation is characterized by a time-constant defined as h^2 / (Ha * k_0), where h is the thickness of the sample, and Ha is the aggregate modulus. This time constant represents the time needed for the peak stress to reduce to 33% of its value when the tissue is subjected to small deformations. Since the samples used in this study had different thickness, a normalized time constant defined as 1/(Ha * k_0) was used to compare the rate of stress relaxation between disc tissues.

Data Analysis

The open-source software FEBio was used to analyze the experimental data (www.febio.org). The curve-fitting process was performed using the optimization algorithm within FEBio. The biphasic-swelling model was implemented in FEBio by adding the deformation dependent osmotic pressure term (Eq. 2) and the biphasic option to a Holmes-Mow matrix. The parameters of the biphasic-swelling model obtained from the curve fitting process were the elastic parameters of the matrix (E, ν, and β) and the parameters of the non-linear permeability (k_0 and M).

The curve fitting was divided in two steps: analyzing the response of the tissue at equilibrium (after swelling and each of the compression ramps) and curve-fitting the stress relaxation curves for all the compression ramps. In the equilibrium analysis, the swelling stretch and the elastic properties (E, ν, β) were determined by satisfying the equilibrium condition between the osmotic pressure, stress in the matrix and applied stress (this procedure is explained in detail in (Cortes and Elliott, 2011; Cortes et al., 2013). In the analysis of stress relaxation curves, the permeability parameters (k_0 and M) were calculated by curve-fitting the biphasic-swelling model. To calculate the effect of swelling on the elastic and permeability properties of the tissue, the measured parameters were compared to those obtained by curve-fitting the experimental data using a biphasic model (without swelling).

Statistical Analysis

All of the parameters (E, ν, β, K_0, M, GAG) were evaluated for differences with respect to tissue type (NP, CEP, AF) using a Kruskal-Wallis test followed by a Dunn's comparison post-test. There was no significant difference between AF tissue location (PAF, OAF, IAF) for any of the measured parameters; therefore, the parameters from those locations were pooled.

RESULTS

Composition

There was no significant difference between the GAG content of tested samples and adjacent tissue (Table 2). However, the water content was higher in the tested samples. This indicates that GAG leaching was negligible, but samples were hydrated during the test. Glycosaminoglycan content (samples) was highest in the NP at 32%/dry weight, whereas the AF was the lowest at 6%/dry weight and the CEP was 14%/dry weight. The water content (82-84%) was similar for the NP and AF and the CEP water was lower (75%). The average fixed charge density, calculated from these compositional parameters, was highest in the NP (317 mM) and lowest in the AF (48.1 mM) (Table 2).

Swelling stretch

The swelling stretch was not different between the disc regions (AF: 1.28±0.16; NP: 1.73±0.74; CEP: 1.29±0.26), with a total average of 1.42. The relative uniformity in swelling stretch could be caused by the high CEP modulus that may have constrained the swelling deformations.

Biphasic-Swelling properties

The elastic parameters were calculated using the optimization routine in FEBio applied to the experimental equilibrium response of each of the compression ramps. The optimization procedure was excellent, with less than 4% average difference in the equilibrium stress between the model fit and the experimental data. The aggregate modulus (Ha) of the matrix was higher in the CEP (390 kPa) compared to the NP (100 kPA) or AF (30 kPa) (Figure 2a). It is important to note that the aggregate modulus (Figure 2a) and the Young's modulus (Table 2) correspond to the uncharged matrix and does not include the contribution of osmotic pressure, which is a separate term in the biphasic-swelling model. Since confined compression was applied perpendicular to AF fibers, the modulus presented in this study represents that of the extra-fibrillar matrix; while for the NP and CEP, the modulus resents all their solid components. The Poisson's ratio (ν=0.18) was not different between the regions ($p = 0.22$).

The permeability parameters were calculated using the optimization routine in FEBio applied to the transient response the compression ramps. The optimization procedure was good, with less than a 10% difference in the peak stress between the model fit and the experimental data (Figure 3). The permeability was very different across tissues regions, with the AF permeability (80 E^{-4} mm^4/Ns) higher than the NP and CEP (6-7 E^{-4} mm^4/Ns) (Figure 2b, note log scale). Although the permeability was different with region, the time-

constant (3000 sec) for the stress relaxation was similar for all the disc tissues. This likely occurs due to the contribution of the modulus, which has the opposite spatial variation compared to the permeability. All the average parameters for the biphasic-swelling model are presented in Table 2.

Standard biphasic properties (without osmotic swelling)

The standard biphasic model, in which swelling is not modeled separately but is combined into solid matrix, was fit to the experimental data. This analysis was performed to evaluate the contribution of swelling on the tissue properties and for comparison to previously published data that use the standard biphasic model. When the confined compression data was analyzed with a biphasic model, the modulus was higher because it includes the contribution of osmotic pressure (Table 3). The permeability of the NP and AF were also higher than that obtained considering swelling of the tissue (Table 3), probably due to differences in the reference configurations.

DISCUSSION

The aim of this study was to measure the human lumbar disc AF, NP, and CEP biphasic-swelling properties to serve as benchmarks for tissues engineering replacements. Strengths of this study are that properties are measured using consistent experimental protocols and analysis of the swelling produced by the GAGs was included. Additionally, human CEP properties are reported for the first time. This analysis showed differences of the elastic modulus, permeability, and fixed charged density between disc tissues. Interestingly, parameters such as swelling stretch and stress-relaxation time-constant were similar across disc tissues.

An important characteristic of this study is that swelling stretch caused by the osmotic pressure was considered in the measurement of mechanical properties. This was accomplished by performing the swelling experiment before the application of the compression ramps. The analysis of the equilibrium (Equation 1) after the swelling period showed that tensile matrix stress is present for all the disc tissues including the CEP and NP. In the case of AF, there was no applied stress during the swelling period (free swelling), which clearly indicates that the osmotic pressure was equilibrated by a tensile matrix stress. For the CEP and NP, the equilibrium condition (equation 1) indicates that the matrix stress must be positive (tension) since the osmotic pressure was higher than the applied stress measured at the end of the swelling period. Consequently, a swelling stretch larger than 1.0 was calculated for the NP and CEP. Since there is no change in volume during the isometric swelling of CEP and NP samples, the calculated tensile matrix stress and stretch may represent the in-situ conditions of these tissues, i.e., tensile matrix stress may be present in the CEP and NP during physiological conditions. Experimental and numerical studies of articular cartilage have shown that tensile matrix stress is produced by the osmotic pressure (Ateshian et al., 2009; Chahine et al., 2004; Nagel and Kelly, 2012).

The effect of swelling on the calculation of disc mechanical properties can be observed by the differences between biphasic-swelling properties (Table 2) and biphasic properties (Table 3). As expected, the aggregate and Young's moduli are lower for the biphasic-

swelling properties since the osmotic pressure is considered separately. The permeability is also lower for the biphasic-swelling model, probably due to differences in reference configuration. For the standard biphasic model, the reference configuration (zero deformation) is assumed as the beginning of the first ramp. Conversely, for the biphasic-swelling model, the solid matrix is stretched at the beginning of the first ramp. This indicates that the reference configuration for the biphasic-swelling model is ‘compressed’ compared that of the biphasic model. This may explain the lower values of permeability for the biphasic-swelling model.

Important differences in biphasic-swelling properties between the individual disc tissues were observed (Figure 2, Table 2). The CEP had the highest aggregate and Young's moduli, which may be related to the higher compressive loads transmitted through the core of the disc. As higher fluid pressures are present in the center of the disc, the higher modulus in the NP and CEP may contribute to resist such forces. Permeability was higher in the AF compared to the NP and CEP. The differences in permeability between disc tissues may have important implications on the mechanical behavior and transport properties of the disc. Lower permeability of the NP and CEP contributes to increase the fluid pressurization of the central part of the disc which is important to carry compressive loading through the spine. Higher permeability of the AF may indicate enhanced fluid flow. However, the distance from the NP to the OAF is larger than to the vertebral endplate, so although fluid flow is ‘easier’ it must travel further to reach the central NP radially from the OAF. Numerical studies are warranted to analyze the effects of regional variation of permeability on the transport to and from the NP (Grunhagen et al., 2011; Jackson et al., 2011).

Although the permeability and the total modulus were different for all the disc tissues, the normalized relaxation time constant was similar for all tissues. This observation is very important since it implies that all the disc tissues dissipate the interstitial fluid pressure at the same rate. The swelling stretch was also similar for all tissues. Differences in normalized relaxation time constant or the swelling stretch could cause stress concentrations in the disc if tissue regions deformed at different rates in response to external or osmotic loads. Therefore, uniformity of swelling deformations could be a consequence of adaptation to avoid localized stress concentration. Indeed, the disc appears to maintain a balance wherein regions with higher GAG content (NP, CEP) have a correspondingly high matrix modulus to restrain excessive swelling and produce conformity in mechanical response between individual disc regions.

Some of the parameters measured in this study can be evaluated within the context of previously published reports on human disc tissues. The glycosaminoglycan and water content reported in this study were similar to previous reported measurements of healthy intervertebral discs (GAG content, NP: 32%, AF: 6%, CEP: 14% of dry weight; water content: NP: 89%, AF: 81%, CEP: 75% of wet weight) (Adams and Muir, 1976; Eyre, 1979; Johannessen and Elliott, 2005; Roberts et al., 1989). However, the water content of the AF measured in this study (81%) was higher than previously reported (50%) (Adams and Muir, 1976). This large difference may have been caused by the initial free swelling that was part of the protocol of the AF and the inclusion of samples from the inner AF. Although the NP had the highest GAG content, the CEP had the highest fixed charge density due to its lower

water content. The values of AF permeability found in this study were in the range of values reported in the literature (1.5-130 × 10^{-16} m^4/Ns), although this range is quite large (Best et al., 1994; Gu et al., 1999; Iatridis et al., 1998; Johannessen and Elliott, 2005; Klisch and Lotz, 2000). The values obtained in this study are closer to those reported by Gu et al., (Gu et al., 1999) (19.2 × 10^{-16} m^4/Ns) where direct permeation experiments were used to measure the permeability. The NP permeability measured in this study was lower than previously reported (Johannessen and Elliott, 2005). Although the prior study also performed a confined compression experiment, a linear model was used to analyze the experiments. There are no values reported in the literature for the permeability of human CEP. The biphasic-swelling modulus values presented in this study do not include the contribution of osmotic pressure and thus cannot be directly compared to moduli in the literature. However, the AF and NP aggregate modulus values for the standard biphasic model (Table 3) are lower than those reported in the past (Table 1). Conversely, the AF biphasic permeability (Table 3) was higher than previous reports (Table 1). These differences may be explained by differences in loading protocols and models used for the data analysis. Although, many important studies have measured elastic, permeability and swelling properties of animal intervertebral disc tissues (Barbir et al., 2010; Heneghan and Riches, 2008; Hongo et al., 2008; MacLean et al., 2007; Périé et al., 2005; Perie et al., 2006; Recuerda et al., 2012; Setton et al., 1993), differences in size, shape, and loading conditions can limit the application of these properties as benchmarks for functional tissue engineering.

The aim of functional tissue engineering is to repair and replace tissues that have a biomechanical function, i.e., connective orthopaedic tissues. Therefore, engineered disc replacements must be designed to achieve similar properties to healthy disc tissues for both function in the joint and to provide mechanical signal to the residing cells. Functional tissue engineering of the intervertebral disc has focused on replacements for the NP, AF, and disc-like constructs (Bowles et al., 2012, 2011; Foss et al., 2014; Hu et al., 2012; Hudson et al., 2013; Iatridis et al., 2013; Jin et al., 2013; Mizuno et al., 2006; Nerurkar et al., 2010b, 2009; O'Halloran and Pandit, 2007; Sasson et al., 2012; Silva-Correia et al., 2011; Strange and Oyen, 2012). Tissue engineering of the AF has mainly focused on replicating its structural and tensile properties (Hudson et al., 2013; Jin et al., 2013; Nerurkar et al., 2009). However, limited data is available on permeability and compressional properties. For NP replacements, the compression modulus is usually similar to that reported to NP; but, the permeability is higher than the values here (Foss et al., 2014; Hu et al., 2012; Sasson et al., 2012; Silva-Correia et al., 2011; Strange and Oyen, 2012). Similarly, the permeability of a whole engineered disc was reported to be 5×10^{-14} m^4/Ns, which is larger than any of the disc tissues (Mizuno et al., 2006). Although a higher permeability may facilitate transport of nutrients and metabolites to the cells, it also will allow for faster exudation of interstitial water, lower hydraulic pressure, and higher stress in the scaffold/matrix under compressive loading. Replicating the low permeability of the NP and CEP and achieving cell viability in this tissue impose a challenge for tissue engineering of disc replacements

The parameters measured here are very important for structural finite element models of the disc's mechanical behavior. Numerical studies on the concentration of nutrients and metabolites heavily depend on the transport properties used in the simulations (Grunhagen et al., 2011; Shirazi-Adl et al., 2010). Tissue engineering of the intervertebral disc can greatly

benefit from these types of numerical studies. Concentration of glucose, oxygen, growth factors, and other metabolites can be simulated for different material properties and loading conditions as it is being done for engineered articular cartilage (Lin et al., 2013; Nims et al., 2013; Raimondi et al., 2011). Hence, properties of the engineered tissue can be modified to produce conditions more favorable for cell survival and physiology.

In conclusion, this study measured the elastic properties, permeability, and swelling properties of human disc tissues, which are important for tissue engineering applications and for structural finite element models of the disc. For tissue engineering, disc replacements should be designed to achieve properties similar to healthy disc tissues for both joint function and for cell mechanotransduction. Moreover, disc tissue engineering can benefit from numerical studies of transport, where the concentration of glucose, oxygen, growth factors, and other moieties can be simulated under various material property and loading conditions. Using such models the engineered tissue can be developed to produce conditions more favorable for cell survival and function.

Acknowledgments

This study was funded by NIH (R01AR050052 and R21AR061751). We are also grateful to NDRI (National Disease Research Interchange) for human tissues and to the developers of the open source software FEBio (www.febio.org).

REFERENCES

Adams MA, Dolan P. Intervertebral disc degeneration: evidence for two distinct phenotypes. J. Anat. 2012; 221:497–506. [PubMed: 22881295]

Adams MA, Roughley PJ. What is intervertebral disc degeneration, and what causes it? Spine. 2006; 31:2151–2161. [PubMed: 16915105]

Adams P, Muir H. Qualitative changes with age of proteoglycans of human lumbar discs. Ann. Rheum. Dis. 1976; 35:289–296. [PubMed: 135533]

Ateshian GA, Rajan V, Chahine NO, Canal CE, Hung CT. Modeling the matrix of articular cartilage using a continuous fiber angular distribution predicts many observed phenomena. J. Biomech. Eng. 2009; 131:061003. [PubMed: 19449957]

Barbir A, Michalek AJ, Abbott RD, Iatridis JC. Effects of enzymatic digestion on compressive properties of rat intervertebral discs. J. Biomech. 2010; 43:1067–1073. [PubMed: 20116063]

Best BA, Guilak F, Setton LA, Zhu W, Saed-Nejad F, Ratcliffe A, Weidenbaum M, Mow VC. Compressive mechanical properties of the human anulus fibrosus and their relationship to biochemical composition. Spine. 1994; 19:212–221. [PubMed: 8153833]

Bowles RD, Gebhard HH, Dyke JP, Ballon DJ, Tomasino A, Cunningham ME, Härtl R, Bonassar LJ. Image-based tissue engineering of a total intervertebral disc implant for restoration of function to the rat lumbar spine. NMR Biomed. 2012; 25:443–451. [PubMed: 21387440]

Bowles RD, Gebhard HH, Härtl R, Bonassar LJ. Tissue-engineered intervertebral discs produce new matrix, maintain disc height, and restore biomechanical function to the rodent spine. Proc. Natl. Acad. Sci. U. S. A. 2011; 108:13106–13111. [PubMed: 21808048]

Chahine NO, Wang CC-B, Hung CT, Ateshian GA. Anisotropic strain-dependent material properties of bovine articular cartilage in the transitional range from tension to compression. J. Biomech. 2004; 37:1251–1261. [PubMed: 15212931]

Cortes DH, Elliott DM. Extra-fibrillar matrix mechanics of annulus fibrosus in tension and compression. Biomech. Model. Mechanobiol. 2011

Cortes DH, Han WM, Smith LJ, Elliott DM. Mechanical properties of the extra-fibrillar matrix of human annulus fibrosus are location and age dependent. J. Orthop. Res. Off. Publ. Orthop. Res. Soc. 2013

Cortes, DH.; Elliott, DM. The Intervertebral Disc: Overview of Disc Mechanics.. In: Shapiro, IM.; Risbud, MV., editors. The Intervertebral Disc. Springer; Vienna: 2014. p. 17-31.

Ehlers W, Karajan N, Markert B. An extended biphasic model for charged hydrated tissues with application to the intervertebral disc. Biomech. Model. Mechanobiol. 2009; 8:233–251. [PubMed: 18661285]

Eyre DR. Biochemistry of the intervertebral disc. Int. Rev. Connect. Tissue Res. 1979; 8:227–291. [PubMed: 389859]

Foss BL, Maxwell TW, Deng Y. Chondroprotective supplementation promotes the mechanical properties of injectable scaffold for human nucleus pulposus tissue engineering. J. Mech. Behav. Biomed. Mater. 2014; 29:56–67. [PubMed: 24055794]

Freeman AL, Buttermann GR, Beaubien BP, Rochefort WE. Compressive properties of fibrous repair tissue compared to nucleus and annulus. J. Biomech. 2013; 46:1714–1721. [PubMed: 23643028]

Galbusera F, Schmidt H, Noailly J, Malandrino A, Lacroix D, Wilke H-J, Shirazi-Adl A. Comparison of four methods to simulate swelling in poroelastic finite element models of intervertebral discs. J. Mech. Behav. Biomed. Mater. 2011; 4:1234–1241. [PubMed: 21783132]

Grunhagen T, Shirazi-Adl A, Fairbank JCT, Urban JPG. Intervertebral disk nutrition: a review of factors influencing concentrations of nutrients and metabolites. Orthop. Clin. North Am. 2011; 42:465–477. vii. [PubMed: 21944584]

Gu WY, Mao XG, Foster RJ, Weidenbaum M, Mow VC, Rawlins BA. The anisotropic hydraulic permeability of human lumbar anulus fibrosus. Influence of age, degeneration, direction, and water content. Spine. 1999; 24:2449–2455. [PubMed: 10626306]

Guerin HL, Elliott DM. Quantifying the contributions of structure to annulus fibrosus mechanical function using a nonlinear, anisotropic, hyperelastic model. J. Orthop. Res. Off. Publ. Orthop. Res. Soc. 2007; 25:508–516.

Guo Z, Shi X, Peng X, Caner F. Fibre-matrix interaction in the human annulus fibrosus. J. Mech. Behav. Biomed. Mater. 2012; 5:193–205. [PubMed: 22100094]

Han WM, Nerurkar NL, Smith LJ, Jacobs NT, Mauck RL, Elliott DM. Multi-scale Structural and Tensile Mechanical Response of Annulus Fibrosus to Osmotic Loading. Ann. Biomed. Eng. 2012

Heneghan P, Riches PE. Determination of the strain-dependent hydraulic permeability of the compressed bovine nucleus pulposus. J. Biomech. 2008; 41:903–906. [PubMed: 18164714]

Holmes MH, Mow VC. The nonlinear characteristics of soft gels and hydrated connective tissues in ultrafiltration. J. Biomech. 1990; 23:1145–1156. [PubMed: 2277049]

Hongo M, Gay RE, Hsu J-T, Zhao KD, Ilharreborde B, Berglund LJ, An K-N. Effect of multiple freeze-thaw cycles on intervertebral dynamic motion characteristics in the porcine lumbar spine. J. Biomech. 2008; 41:916–920. [PubMed: 18078942]

Hu J, Chen B, Guo F, Du J, Gu P, Lin X, Yang W, Zhang H, Lu M, Huang Y, Xu G. Injectable silk fibroin/polyurethane composite hydrogel for nucleus pulposus replacement. J. Mater. Sci. Mater. Med. 2012; 23:711–722. [PubMed: 22231270]

Hudson KD, Alimi M, Grunert P, Härtl R, Bonassar LJ. Recent advances in biological therapies for disc degeneration: tissue engineering of the annulus fibrosus, nucleus pulposus and whole intervertebral discs. Curr. Opin. Biotechnol. 2013

Iatridis JC, Kumar S, Foster RJ, Weidenbaum M, Mow VC. Shear mechanical properties of human lumbar annulus fibrosus. J. Orthop. Res. Off. Publ. Orthop. Res. Soc. 1999; 17:732–737.

Iatridis JC, Nicoll SB, Michalek AJ, Walter BA, Gupta MS. Role of biomechanics in intervertebral disc degeneration and regenerative therapies: what needs repairing in the disc and what are promising biomaterials for its repair? Spine J. Off. J. North Am. Spine Soc. 2013; 13:243–262.

Iatridis JC, Setton LA, Foster RJ, Rawlins BA, Weidenbaum M, Mow VC. Degeneration affects the anisotropic and nonlinear behaviors of human anulus fibrosus in compression. J. Biomech. 1998; 31:535–544. [PubMed: 9755038]

Iatridis JC, Setton LA, Weidenbaum M, Mow VC. The viscoelastic behavior of the non-degenerate human lumbar nucleus pulposus in shear. J. Biomech. 1997; 30:1005–1013. [PubMed: 9391867]

Jackson AR, Huang C-YC, Brown MD, Gu WY. 3D finite element analysis of nutrient distributions and cell viability in the intervertebral disc: effects of deformation and degeneration. J. Biomech. Eng. 2011; 133:091006. [PubMed: 22010741]

Jacobs NT, Smith LJ, Han WM, Morelli J, Yoder JH, Elliott DM. Effect of orientation and targeted extracellular matrix degradation on the shear mechanical properties of the annulus fibrosus. J. Mech. Behav. Biomed. Mater. 2011; 4:1611–1619. [PubMed: 22098863]

Jin L, Shimmer AL, Li X. The challenge and advancement of annulus fibrosus tissue engineering. Eur. Spine J. Off. Publ. Eur. Spine Soc. Eur. Spinal Deform. Soc. Eur. Sect. Cerv. Spine Res. Soc. 2013; 22:1090–1100.

Johannessen W, Elliott DM. Effects of degeneration on the biphasic material properties of human nucleus pulposus in confined compression. Spine. 2005; 30:E724–729. [PubMed: 16371889]

Klisch SM, Lotz JC. Application of a fiber-reinforced continuum theory to multiple deformations of the annulus fibrosus. J. Biomech. 1999; 32:1027–1036. [PubMed: 10476841]

Klisch SM, Lotz JC. A special theory of biphasic mixtures and experimental results for human annulus fibrosus tested in confined compression. J. Biomech. Eng. 2000; 122:180–188. [PubMed: 10834159]

Lee K-I, Moon S-H, Kim H, Kwon U-H, Kim H-J, Park S-N, Suh H, Lee H-M, Kim H-S, Chun H-J, Kwon I-K, Jang J-W. Tissue engineering of the intervertebral disc with cultured nucleus pulposus cells using atelocollagen scaffold and growth factors. Spine. 2012; 37:452–458. [PubMed: 22037529]

Lin T-H, Jhang H-Y, Chu F-C, Chung CA. Computational modeling of nutrient utilization in engineered cartilage. Biotechnol. Prog. 2013; 29:452–462. [PubMed: 23297021]

MacLean JJ, Owen JP, Iatridis JC. Role of endplates in contributing to compression behaviors of motion segments and intervertebral discs. J. Biomech. 2007; 40:55–63. [PubMed: 16427060]

Mizuno H, Roy AK, Zaporojan V, Vacanti CA, Ueda M, Bonassar LJ. Biomechanical and biochemical characterization of composite tissue-engineered intervertebral discs. Biomaterials. 2006; 27:362–370. [PubMed: 16165204]

Nagel T, Kelly DJ. Apparent behaviour of charged and neutral materials with ellipsoidal fibre distributions and cross-validation of finite element implementations. J. Mech. Behav. Biomed. Mater. 2012; 9:122–129. [PubMed: 22498290]

Nerurkar NL, Baker BM, Sen S, Wible EE, Elliott DM, Mauck RL. Nanofibrous biologic laminates replicate the form and function of the annulus fibrosus. Nat. Mater. 2009; 8:986–992. [PubMed: 19855383]

Nerurkar NL, Elliott DM, Mauck RL. Mechanical design criteria for intervertebral disc tissue engineering. J. Biomech. 2010a; 43:1017–1030. [PubMed: 20080239]

Nerurkar NL, Han W, Mauck RL, Elliott DM. Homologous structure-function relationships between native fibrocartilage and tissue engineered from MSC-seeded nanofibrous scaffolds. Biomaterials. 2011; 32:461–468. [PubMed: 20880577]

Nerurkar NL, Sen S, Huang AH, Elliott DM, Mauck RL. Engineered disc-like angle-ply structures for intervertebral disc replacement. Spine. 2010b; 35:867–873. [PubMed: 20354467]

Nims RJ, Cigan AD, Albro MB, Hung CT, Ateshian GA. Synthesis rates and binding kinetics of matrix products in engineered cartilage constructs using chondrocyte-seeded agarose gels. J. Biomech. 2013

O'Connell GD, Sen S, Elliott DM. Human annulus fibrosus material properties from biaxial testing and constitutive modeling are altered with degeneration. Biomech. Model. Mechanobiol. 2012; 11:493–503. [PubMed: 21748426]

O'Halloran DM, Pandit AS. Tissue-engineering approach to regenerating the intervertebral disc. Tissue Eng. 2007; 13:1927–1954. [PubMed: 17518718]

Périé D, Korda D, Iatridis JC. Confined compression experiments on bovine nucleus pulposus and annulus fibrosus: sensitivity of the experiment in the determination of compressive modulus and hydraulic permeability. J. Biomech. 2005; 38:2164–2171. [PubMed: 16154403]

Perie D, MacLean J, Owen J, Iatridis J. Correlating material properties with tissue composition in enzymatically digested bovine annulus fibrosus and nucleus pulposus tissue. Ann. Biomed. Eng. 2006; 34:769–777. [PubMed: 16598654]

Raimondi MT, Causin P, Mara A, Nava M, Laganà M, Sacco R. Breakthroughs in computational modeling of cartilage regeneration in perfused bioreactors. IEEE Trans. Biomed. Eng. 2011; 58:3496–3499. [PubMed: 21813363]

Recuerda M, Périé D, Gilbert G, Beaudoin G. Assessment of mechanical properties of isolated bovine intervertebral discs from multi-parametric magnetic resonance imaging. BMC Musculoskelet. Disord. 2012; 13:195. [PubMed: 23061966]

Roberts S, Menage J, Urban JP. Biochemical and structural properties of the cartilage end-plate and its relation to the intervertebral disc. Spine. 1989; 14:166–174. [PubMed: 2922637]

Sasson A, Patchornik S, Eliasy R, Robinson D, Haj-Ali R. Hyperelastic mechanical behavior of chitosan hydrogels for nucleus pulposus replacement-experimental testing and constitutive modeling. J. Mech. Behav. Biomed. Mater. 2012; 8:143–153. [PubMed: 22402161]

Sen S, Jacobs NT, Boxberger JI, Elliott DM. Human Annulus Fibrosus Dynamic Tensile Modulus Increases with Degeneration. Mech. Mater. Int. J. 2012; 44:93–98.

Setton LA, Zhu W, Weidenbaum M, Ratcliffe A, Mow VC. Compressive properties of the cartilaginous end-plate of the baboon lumbar spine. J. Orthop. Res. Off. Publ. Orthop. Res. Soc. 1993; 11:228–239.

Shirazi-Adl A, Taheri M, Urban JPG. Analysis of cell viability in intervertebral disc: Effect of endplate permeability on cell population. J. Biomech. 2010; 43:1330–1336. [PubMed: 20167323]

Silva-Correia J, Oliveira JM, Caridade SG, Oliveira JT, Sousa RA, Mano JF, Reis RL. Gellan gum-based hydrogels for intervertebral disc tissue-engineering applications. J. Tissue Eng. Regen. Med. 2011; 5:e97–107. [PubMed: 21604382]

Strange DGT, Oyen ML. Composite hydrogels for nucleus pulposus tissue engineering. J. Mech. Behav. Biomed. Mater. 2012; 11:16–26. [PubMed: 22658151]

Urban JPG, Roberts S. Degeneration of the intervertebral disc. Arthritis Res. Ther. 2003; 5:120–130. [PubMed: 12723977]

Wagner DR, Lotz JC. Theoretical model and experimental results for the nonlinear elastic behavior of human annulus fibrosus. J. Orthop. Res. Off. Publ. Orthop. Res. Soc. 2004; 22:901–909.

Wagner DR, Reiser KM, Lotz JC. Glycation increases human annulus fibrosus stiffness in both experimental measurements and theoretical predictions. J. Biomech. 2006; 39:1021–1029. [PubMed: 15878594]

Wilson W, van Donkelaar CC, Huyghe JM. A comparison between mechano-electrochemical and biphasic swelling theories for soft hydrated tissues. J. Biomech. Eng. 2005; 127:158–165. [PubMed: 15868798]

Wu HC, Yao RF. Mechanical behavior of the human annulus fibrosus. J. Biomech. 1976; 9:1–7. [PubMed: 1249075]

Xin H, Zhang C, Wang D, Shi Z, Gu T, Wang C, Wu J, Zhang Y, He Q, Ruan D. Tissue-engineered allograft intervertebral disc transplantation for the treatment of degenerative disc disease: experimental study in a beagle model. Tissue Eng. Part A. 2013; 19:143–151. [PubMed: 22849557]

Zhu Q, Jackson AR, Gu WY. Cell viability in intervertebral disc under various nutritional and dynamic loading conditions: 3d finite element analysis. J. Biomech. 2012; 45:2769–2777. [PubMed: 23040882]

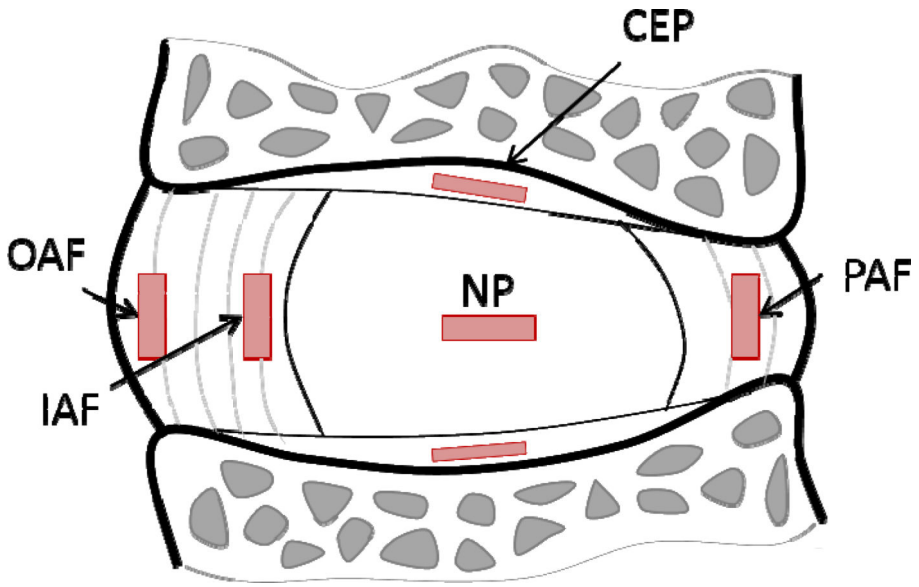

Figure 1.

Sagittal section of the intervertebral disc showing the location of teh confined compression samples (discs of 4mm in diameter). OAF: outer-anterior annulus fibrosus, IAF: inner-anterior annulus fibrosus, NP: nucleus pulposus, CEP: cartilaginous endplate.

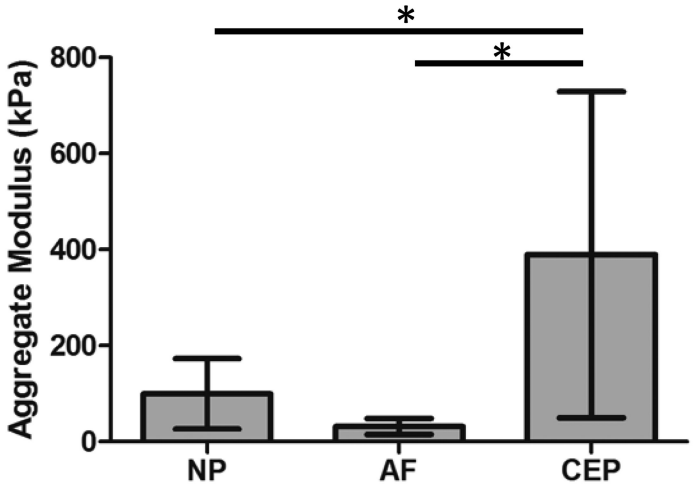

a)

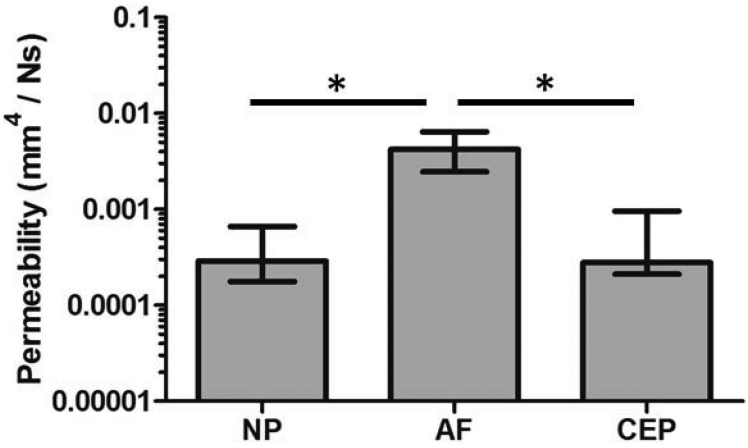

b)

Figure 2.

Properties (median and interquartile range) obtained using the biphasic swelling model were location dependent: A) the aggregate modulus was highest at the CPE, B) the permeability was highest in the AF. Note the logarithmic scale. *p<0.05. NP = nucleus pulposus, AF = annulus fibrosus, CEP = cartilaginous endplate.

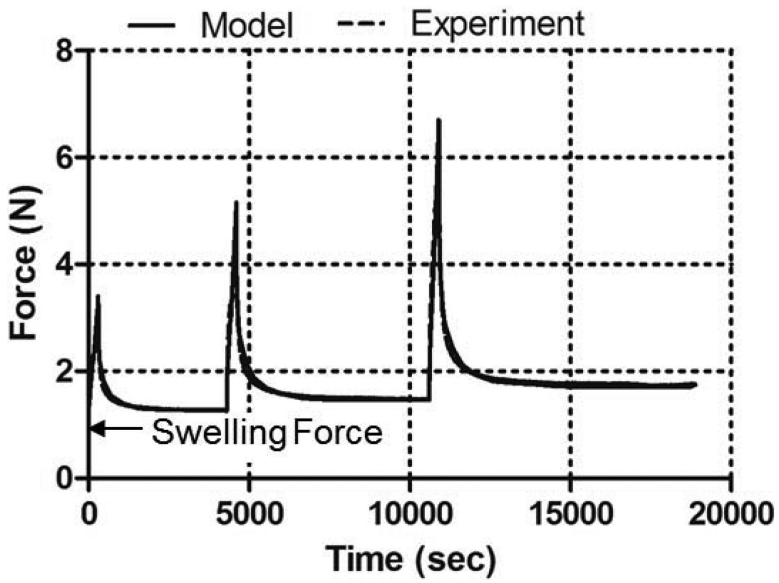

Figure 3.

Representative plot of the curve-fitting of the transient response of the nucleus pulposus during the compression ramps. Notice that the experimental curve and the model prediction do not start at the origin, but at the swelling force indicated with an arrow.

Table 1

Experimental elastic and permeability parameters of the matrix of human intervertebral disc tissues reported in the literature.

	NP	AF	CEP
Ha (kPa)	1010 [1]	380 [3]	--
		116 [4]	
	4000-6000 [10]	560 [5]	
		29.9 [*6]	
		5000-7000 [10]	
$\mathbf{k_0} \times 10^{-16}$ (m^4/Ns)	14 [1]	2.4 [3]	--
		130 [4]	
		19.2 [7]	
		2.1 [8]	
μ (kPa)	10.5 [2]	110 [9]	--
FCD (mM)	--	46.5 [6]	--

NP: nucleus pulposus, AF: annulus fibrosus, CEP: cartilaginous endplate, Ha: aggregate modulus, k_0: permeability at the reference configuration, μ: shear modulus, FCD: fixed charge density.

[*] (obtained with the biphasic-swelling model).

[1] (Johannessen and Elliott, 2005)

[2] (Iatridis et al., 1997)

[3] (Best et al., 1994)

[4] (Klisch and Lotz, 2000)

[5] (Iatridis et al., 1998)

[6] (Cortes et al., 2013)

[7] (Gu et al., 1999)

[8] (Iatridis et al., 1998)

[9] (Iatridis et al., 1999)

[10] (Freeman et al., 2013).

Table 2

Properties (average ± standard deviation) of the biphasic-swelling model for individual disc tissues.

	NP	AF	CEP
E (kPa)	64.9 ± 44.1	25.0 ± 21.6	305.2 ± 223.4
ν	0.24 ± 0.14	0.16 ± 0.14	0.18 ± 0.14
Ha (kPa)	99.7 ± 73.3	31.4 ± 16.5	389.4 ± 339.5
β	0.95	3.3 ± 4.2	0.29 ± 0.5
$\mathbf{k_0} \times 10^{-4}$ (mm^4/Ns)	5.5 ± 7.8	64 ± 76	5.6 ± 5.1
M	1.92	4.8 ± 3.5	3.79 ± 2.61
GAG (% dry weight)*	32.4 ± 16.6	5.9 ± 2.4	14.0 ± 5.5
GAG (% dry weight)**	44.3 ± 19.52	--	14.7 ± 6.9
Water (% wet weight)*	89.7 ± 5.6	81.4 ± 4.3	75.4 ± 6.6
Water (% wet weight)**	78.6 ± 2.9	--	59.7 ± 6.8
FCD (mM)***	128.7 ± 88.1	46.5 ± 14.5	220.1 ± 109.4
Normalized Time Constant	2127 ± 1244	4487 ± 3697	2481 ± 2559

NP: nucleus pulposus, AF: annulus fibrosus, CEP: cartilaginous endplate, E: Young's modulus, ν: Poisson's ratio, Ha: aggregate modulus, β: non-linear parameter of the Holmes-Mow model, k_0: permeability at the reference configuration, M: non-linear parameter of the permeability, GAG: glycosaminoglycan content, μ: shear modulus, FCD: fixed charge density.

* Measured in the tested sample

** Measured in the adjacent tissue

*** NP and CEP properties calculated using average GAG and water of tested samples and adjacent tissue.

Table 3

Parameters of the biphasic model for different disc tissues.

	NP	AF	CEP
E (kPa)	202 ± 48	21.7 ± 22.7	521.8 ± 345
ν	0.36 ± 0.07	0.26 ± 0.2	0.38 ± 0.14
Ha (kPa)	466.5 ± 281.5	34.2 ± 37.0	1402.5 ± 709
β	1.46 ± 1.78	3.18 ± 1.56	0.0028 ± 0.008
$\mathbf{k_0} \times 10^{-4}$ (mm^4/Ns)	18.7 ± 14.8	180 ± 127	5.5 ± 4.8
M	4.8 ± 3.0	6.80 ± 2.62	0.22 ± 0.31

NP: nucleus pulposus, AF: annulus fibrosus, CEP: cartilaginous endplate, E: Young's modulus, ν: Poisson's ratio, Ha: aggregate modulus, β: non-linear parameter of the Holmes-Mow model, k_0: permeability at the reference configuration, M: non-linear parameter of the permeability.